

1 ***Bradyrhizobium diazoefficiens* USDA110 nodulation of *Aeschynomene afraspera* is
2 associated with atypical terminal bacteroid differentiation and suboptimal symbiotic
3 efficiency**

4

5 Running title: *Bradyrhizobium* differentiation in *Aeschynomene*

6

7 Quentin Nicoud^{1*}, Florian Lamouche^{1*}, Anaïs Chaumeret¹, Thierry Balliau², Romain Le Bars¹,
8 Mickaël Bourge¹, Fabienne Pierre¹, Florence Guérard³, Erika Sallet⁴, Solenn Tuffigo¹, Olivier
9 Pierre¹, Yves Dessaix¹, Françoise Gilard³, Bertrand Gakière³, Istvan Nagy^{5,6}, Attila Kereszt^{5,6},
10 Michel Zivy², Peter Mergaert¹, Benjamin Gourion⁴, Benoit Alunni^{1#}

11

12 ¹ Université Paris-Saclay, CEA, CNRS, Institute for Integrative Biology of the Cell (I2BC),
13 Gif-sur-Yvette, 91198, France

14 ² PAPPSO, GQE-Le Moulon, INRAE, CNRS, AgroParisTech, Paris-Saclay University, 91190
15 Gif-sur-Yvette, France

16 ³ SPOmics platform, Institute of Plant Sciences Paris-Saclay (IPS2), CNRS, INRAE,
17 Universities Paris-Saclay, Evry and de Paris, Batiment 630, 91405 Orsay, France

18 ⁴ LIPM, Université de Toulouse, INRAE, CNRS, Castanet-Tolosan, France

19 ⁵ Institute of Biochemistry, Hungarian Academy of Sciences, Biological Research Centre, 6726
20 Szeged, Hungary

21 ⁶ Seqomics Biotechnology Ltd., 6782 Mórahalom, Hungary

22

23 * co-first authors

24 # Author to whom correspondence should be addressed: benoit.alunni@i2bc.paris-saclay.fr

25

26

27

28

29

30

31

32

33

34 **Abstract** (max. 250 words)

35 Legume plants can form root organs called nodules where they house intracellular symbiotic
36 rhizobium bacteria. Within nodule cells, rhizobia differentiate into bacteroids, which fix
37 nitrogen for the benefit of the plant. Depending on the combination of host plants and rhizobial
38 strains, the output of rhizobium-legume interactions is varying from non-fixing associations to
39 symbioses that are highly beneficial for the plant. *Bradyrhizobium diazoefficiens* USDA110
40 was isolated as a soybean symbiont but it can also establish a functional symbiotic interaction
41 with *Aeschynomene afraspera*. In contrast to soybean, *A. afraspera* triggers terminal bacteroid
42 differentiation, a process involving bacterial cell elongation, polyploidy and membrane
43 permeability leading to loss of bacterial viability while plants increase their symbiotic benefit.
44 A combination of plant metabolomics, bacterial proteomics and transcriptomics along with
45 cytological analyses was used to study the physiology of USDA110 bacteroids in these two
46 host plants. We show that USDA110 establish a poorly efficient symbiosis with *A. afraspera*,
47 despite the full activation of the bacterial symbiotic program. We found molecular signatures
48 of high level of stress in *A. afraspera* bacteroids whereas those of terminal bacteroid
49 differentiation were only partially activated. Finally, we show that in *A. afraspera*, USDA110
50 bacteroids undergo an atypical terminal differentiation hallmarked by the disconnection of the
51 canonical features of this process. This study pinpoints how a rhizobium strain can adapt its
52 physiology to a new host and cope with terminal differentiation when it did not co-evolve with
53 such a host.

54

55 **Importance** (max 150 words)

56 Legume-rhizobium symbiosis is a major ecological process in the nitrogen cycle,
57 responsible for the main input of fixed nitrogen in the biosphere. The efficiency of this
58 symbiosis relies on the coevolution of the partners. Some legume plants, but not all, optimize

59 their return-on-investment in the symbiosis by imposing on their microsymbionts a terminal
60 differentiation program that increases their symbiotic efficiency but imposes a high level of
61 stress and drastically reduce their viability. We combined multi-omics with physiological
62 analyses to show that the non-natural symbiotic couple formed by *Bradyrhizobium*
63 *diazoefficiens* USDA110 and *Aeschynomene afraspera* is functional but displays a low
64 symbiotic efficiency associated to a disconnection of terminal bacteroid differentiation features.

65 Introduction

66 Nitrogen availability is a major limitation for plant development in many environments,
67 including agricultural settings. To overcome this problem and thrive on substrates presenting a
68 low nitrogen content, crops are heavily fertilized, causing important environmental damage and
69 financial drawbacks^{1,2}. Plants of the legume family acquired the capacity to form symbiotic
70 associations with soil bacteria, the rhizobia, which fix atmospheric nitrogen for the plants'
71 benefit. These symbiotic associations lead to the development of rhizobia-housing root organs
72 called nodules. In these nodules, the rhizobia adopt an intracellular lifestyle and differentiate
73 into bacteroids that convert atmospheric dinitrogen into ammonia and transfer it to the plant.
74 Critical recognition steps occur all along the symbiotic process and define the compatibility of
75 the plant and bacterial partners³. While the mechanisms involved at the early stages of the
76 symbiosis are well described, those of the later stages are much less clear and might affect not
77 only the ability to interact but also the efficiency of the symbiosis (ie. the plant benefit).

78 Nodule-specific Cysteine-Rich (NCR) antimicrobial peptides produced by legumes of the
79 Dalbergioids and Inverted Repeat Lacking Clade (IRLC) were proposed to play a crucial role
80 in the control of host-symbiont specificity at the intracellular stage of the symbiosis⁴. NCR
81 peptides are targeted to the bacteroids where they govern the bacteroid differentiation⁵⁻⁹. In
82 these legumes, the differentiation process entails such profound changes that they suppress the
83 bacteroids' capacity to resume growth and is therefore referred to as terminal bacteroid
84 differentiation (TBD). TBD contrasts with bacteroid formation in legumes that lack NCR genes
85 (eg. soybean), where bacteroids are in a reversible state and can resume growth when released
86 from nodules¹⁰. Specifically, TBD is associated with cell elongation, an increase in bacteroid
87 DNA content through a cell cycle switch toward endoreduplication^{6,9,11}. Furthermore, an
88 increased permeability of the bacteroid envelope also occurs during TBD, most probably due
89 to the interaction of NCR peptides with bacterial membranes^{6,7,10,12}. Together, these alterations

90 of bacteroid physiology are associated to a strongly decreased viability of the differentiated
91 bacteria, that fail to recover growth when extracted from nodules⁶.

92 While many rhizobia have a narrow host range, some species can nodulate a large array of
93 plant species. One of them, *Bradyrhizobium diazoefficiens* USDA110, can trigger functional
94 nodules without TBD on soybean (*Glycine max*), cowpea (*Vigna unguiculata*) or siratro
95 (*Macroptilium atropurpureum*) (Fig 1A-B)¹³. In addition to these species, USDA110 induces
96 also functional nodules on the TBD-inducing legume *Aeschynomene afraspera* (Fig. 1A-C)^{14,15}.
97 However, in *A. afraspera*, USDA110 shows only very limited features that are usually
98 associated with TBD, suggesting that the bacterium might be resistant to the TBD process¹⁶.

99 Herein, we further characterized the bacteroid differentiation in the symbiosis between
100 USDA110 and *A. afraspera*. Our observations, supported by whole-nodule metabolome
101 analysis, indicate that USDA110 is poorly matched for nitrogen fixation with *A. afraspera*. To
102 understand better the adaptation of *B. diazoefficiens* physiology to the *G. max* and *A. afraspera*
103 nodule environment, we used a combination of transcriptomics (RNA-seq) and shotgun
104 proteomics (LC-MS/MS) approaches. Finally, we find that USDA110 undergoes a terminal but
105 atypical bacteroid differentiation in *A. afraspera* with a reduced cell viability and an increased
106 membrane permeability, while cell size and ploidy level remain unchanged.

107

108 **Results**

109 ***B. diazoefficiens* USDA110 is poorly matched with *A. afraspera* for nitrogen fixation**

110 Previous reports indicate that *B. diazoefficiens* USDA110, the model symbiont of soybean,
111 is able to establish a functional nitrogen-fixing symbiosis with *A. afraspera*, a phylogenetically
112 distant host belonging to the Dalbergioid clade, which naturally interacts with photosynthetic
113 rhizobia such as *Bradyrhizobium* sp. ORS285 (Fig. 1A-C)¹⁴⁻¹⁸. To evaluate the efficiency of
114 this symbiosis, nitrogenase activity of USDA110- and ORS285-infected plants and their

115 nitrogen content were determined. Although nitrogenase activity was detected in both types of
116 nodules, it was significantly lower in USDA110-nodulated plants (Fig. 1D). A similar trend is
117 observed for mass gain per nodule mass although this difference is not significant (Fig. 1E).
118 Nitrogen and carbon contents seemed also reduced in USDA110-nodulated plants as compared
119 to ORS285-nodulated plants, reaching levels similar to those of non-inoculated plants (Fig. S1).
120 Accordingly, ORS285-nodulated *A. afraspera* plants display darker green leaves than those
121 interacting with USDA110.

122 Moreover, their shoot/root mass ratio, a metric that reflects the nutritional status of the
123 plant, is reduced in USDA110-nodulated *A. afraspera* plants as compared to ORS285-
124 nodulated plants, indicating that the plant nutritional needs are not fulfilled (Fig. S2)¹⁹. To
125 characterize further this suboptimal symbiosis, we analyzed the whole-nodule metabolome.
126 Soybean nodules infected with USDA110 were used as a reference (Fig. S3). Allantoin, which
127 is known to be the major nitrogen form exported from soybean nodules, is specifically detected
128 in them (Fig. 1F)²⁰. On the contrary, asparagine and glutamine are the principal exported
129 nitrogen compounds in *A. afraspera* nodules and their amount is lower in USDA110-infected
130 nodules as compared to ORS285-infected nodules, indicating a reduced nitrogen fixation by the
131 bacteroids (Fig. 1F)¹⁸.

132 In addition, we find specifically in USDA110-infected *A. afraspera* nodules the
133 accumulation of sucrose, phosphoric acid and ascorbate, and oppositely, a strong reduction in
134 the trehalose content (Fig. 1F, Fig. S3). Sucrose derived from phloem sap is metabolized in
135 nodules to fuel the bacteroids with carbon substrates, usually dicarboxylates. The accumulation
136 of sucrose in nodules indicates a symbiotic dysfunction. Also, the accumulation of phosphoric
137 acid in nodules suggests that nitrogen fixation is not reaching its optimal rate. Ascorbate has
138 been shown to increase nitrogen fixation activity by modulating the redox status of
139 leghemoglobin^{21,22}. Thus, its accumulation in nodules with reduced nitrogen fixation capacity

140 could be a stress response to rescue nitrogen fixation in nodules that do not fix nitrogen
141 efficiently. A trehalose biosynthesis gene is upregulated in ORS285 bacteroids in *A. afraspera*,
142 suggesting that TBD is accompanied by the synthesis of this osmo-protectant disaccharide¹⁷.
143 The lower synthesis in USDA110 bacteroids suggests an altered TBD. Together these data
144 indicate a metabolic disorder in the USDA110-infected nodules, in agreement with USDA110
145 being a suboptimal symbiont of *A. afraspera*.

146

147 **Overview of the USDA110 bacteroid proteomes and transcriptomes**

148 In order to better understand the poor interaction between USDA110 and *A. afraspera*, the
149 bacteroid physiology was analyzed through transcriptome and proteome analysis. The efficient
150 soybean bacteroids and the free-living USDA110 cells cultivated in rich medium (exponential
151 growth phase in aerobic condition) were used as references (Fig. 2A).

152 Prior to quantification of transcript abundance or identification and quantification of protein
153 accumulation, the transcriptome dataset was used to re-annotate the USDA110 genome with
154 the EugenePP pipeline²³. This allowed the definition of 876 new CDS, ranging from 92 to
155 1091bp (median size = 215bp or 71.6 aa) with 11.5% of them having a predicted function or at
156 least a match using InterProScan (IPR). This extends the total number of CDS in the USDA110
157 genome to 9171. Moreover, we also identified 246 ncRNAs, ranging from 49 to 765 bp (median
158 = 76 bp), which were not annotated before. Proteomic evidence could be found for 28 new CDS
159 (3.2% of the new CDS, median size = 97.6 aa). The complete reannotation of the genome is
160 described in Table S1.

161 In the proteome dataset, 1808 USDA110 proteins were identified. Principal component
162 analysis (PCA) of all the replicate samples and sample types revealed their partitioning
163 according to the tested conditions. The first axis of the PCA (40.2% of the observed variance)
164 separates bacteroid profiles from the exponential culture, whereas the second axis separates *G.*

165 *max* bacteroids from *A. afraspera* bacteroids (14.9% of the observed variance; Fig. 2B). The
166 samples of the transcriptome datasets are similarly distributed on the PCA plot, with a first axis
167 explaining 42.6% of the observed variance and a second axis explaining 23.5% of the observed
168 variance (Fig. 2B).

169 Although differences are less pronounced in the proteome dataset than in the transcriptome
170 dataset, COG analysis shows similar profiles across functional categories, except for membrane
171 proteins that are less well identified in proteomics than transcriptomics (Fig. S4). In the
172 transcriptomic dataset, 3150 genes are differentially expressed in at least one condition
173 (differentially expressed genes or DEGs). Among the 1808 proteins identified, 815 show
174 differential accumulation (differentially accumulated proteins or DAPs) and 438 of the cognate
175 genes are also differentially expressed in the transcriptome datasets, whereas 175 DEGs are not
176 DAPs (Fig. 2C).

177 We analyzed the Pearson correlation between transcriptomic and proteomic profiles and
178 found that ~66% of the bacterial functions that show significant differences in both approaches
179 display a high correlation coefficient ($r>0.9$) whereas less than 1% of the functions show strong
180 negative correlation ($r<-0.9$; Fig. 2D). This observation suggests that the transcriptome (which
181 provides a more exhaustive view than the proteome) and the proteome provide a
182 complementary picture of bacterial physiology, and they tend to show a congruent information
183 if we restrict our analysis to the genes with differential accumulation/expression (Fig. 2E).
184 However, there is still around 66% of the DEGs, which were detected by the proteomic analysis,
185 that are not DAPs. Our description of the bacterial functions will be primarily based on the
186 functions that are both DEGs and DAPs, as there is stronger evidence of their modulation in the
187 tested conditions. The transcriptome alone will be used only when proteomics is not
188 informative, for example to analyze regulons and stimulons that have been described previously
189 in USDA110.

190

191 **Symbiotic functions common to both types of USDA110 bacteroids**

192 Among the 815 DAPs, 705 and 699 proteins are significantly differentially accumulated in
193 *G. max* and *A. afraspera* respectively compared to the bacterial culture control. Strikingly, 646
194 proteins are commonly differentially accumulated in both plant nodules (Table S1).

195 In the transcriptomic dataset, 1999 DEGs, representing ~21% of the genome, were
196 identified between the bacterial culture and the bacteroids, regardless of the host. Among them,
197 1076 genes displayed higher expression in nodules (including seven newly annotated ncRNAs
198 and one newly annotated CDS among the 20 differentially expressed genes with highest fold
199 change) and 923 genes were repressed *in planta* (including two newly annotated ncRNAs and
200 two newly annotated CDS among the 20 DEG with highest fold change, Table S1).

201 Restricting the analysis to the bacterial functions that are both differentially expressed
202 (DEG) and differentially accumulated (DAP) *in planta* in both hosts as compared to the
203 bacterial culture identified 222 genes/proteins, 150 being upregulated and 72 being repressed
204 *in planta* respectively (Fig. 3A). Notably, six newly annotated genes are in this gene list
205 including one putative regulator (Bd110_01119) that is induced during symbiosis. Among the
206 functions commonly DEG and DAP *in planta*, only four functions showed opposite trends in
207 proteomics and transcriptomics.

208 The proteome and transcriptome data provided a coherent view of the nitrogen fixation
209 metabolism of *B. diazoefficiens* in the tested conditions. Key enzymes involved in microoxic
210 respiration and nitrogen fixation were detected amongst the proteins having the highest spectra
211 number in the nodule samples (Fig. 3A, Table S1) and the corresponding genes are among the
212 most strongly expressed ones in bacteroids, while almost undetectable in the free-living
213 condition. This includes for instance, the nitrogenase and the nitrogenase reductase subunits,
214 which constitute the nitrogenase enzyme complex responsible for nitrogen conversion into

215 ammonia. They belong to a locus of 21 genes from *blr1743* (*nifD*) to *bll1778* (*ahpC_2*),
216 including the genes involved in nitrogenase cofactor biosynthesis, in electron transport to
217 nitrogenase, and in microaerobic respiration, that are among the highest expressed ones in
218 bacteroids of both host plants, both at the gene and protein expression level. The slightly higher
219 level of the dinitrogenase reductase NifH detected in proteomics was not supported by western
220 blot analysis, which showed apparent similar protein level in both bacteroid conditions (Fig.
221 S5). Strikingly, the two bacteroid types did not show a notable difference in the expression of
222 these genes and proteins, suggesting that the activation of the nitrogen fixation machinery is
223 not a limiting factor underlying the suboptimal efficiency of strain USDA110 in *A. afraspera*
224 nodules.

225 In addition to these expected bacteroid functions, many other proteins were identified that
226 specifically and strongly accumulated in both nodule types. This is the case of the chaperonins
227 GroEL1/GroES1, which are strongly upregulated and reach high gene expression and protein
228 levels in both bacteroids. The upregulation of these chaperonins is remarkable because other
229 GroEL/GroES (4, 5 and 7) proteins are also very strongly accumulated in a constitutive manner.
230 This indicates that bacteroids have a high demand for protein folding, possibly requiring
231 specific GroEL isoforms, a situation reminding the requirement of one out of five GroEL
232 isoforms for symbiosis in *Sinorhizobium meliloti*, the symbiont of *Medicago sativa*^{12,24}.
233 Another example of a bacteroid-specific function is the hydrogenase uptake system, whose gene
234 expression was induced in both bacteroid types from nearly no expression in culture.
235 Hydrogenase subunit HupL_2 (*bll6941*) was found amongst the proteins displaying the highest
236 spectra number in the nodule samples suggesting important electron recycling in bacteroids of
237 the two hosts. Another one is the 1-aminocyclopropane-1-carboxylic acid (ACC) deaminase
238 (*blr0241*), which was also amongst the most strongly accumulated proteins in nodules and was
239 significantly less abundant in free-living USDA110. An outer membrane protein (*bll1872*)

240 belonging to the NifA regulon²⁵ was also strongly induced *in planta*, with a transcript level
241 among the top 10 genes in *A. afraspera*. Additionally, a locus of seven genes (*blr7916-blr7922*)
242 encoding an amidase enzyme and a putative peptide transporter composed of two
243 transmembrane domain proteins, two ATPases and two solute-binding proteins was strongly
244 upregulated in the two bacteroid types, with three protein being also over-accumulated *in planta*
245 (Fig. 3A; Table S1).

246 Oppositely, motility genes encoding flagella subunits (*bll5844-bll5846*), metabolic
247 enzymes and transporter subunits are strongly downregulated during symbiosis and hardly
248 detectable at the protein level *in planta* (Fig. 3A).

249 Taken together, these data show that both bacteroid types display a typical nitrogen fixation-
250 oriented metabolism, with a partial shutdown of housekeeping functions. This indicates that
251 despite the apparent reduced symbiotic efficiency of USDA110 in *A. afraspera* nodules, the
252 bacterium fully expresses its symbiotic program within this non-native host as it does in
253 soybean, its original host. Thus, the sub-optimal functioning of the *A. afraspera* nodules does
254 not seem to come from a bacterial defect to express the symbiotic program, but possibly from
255 an unfavorable host microenvironment or from a lack of metabolic integration of these
256 maladapted partners.

257

258 **Host-specific functions**

259 Comparison of the *A. afraspera* and *G. max* bacteroids revealed also significant differences
260 in the proteomes and transcriptomes. At the transcriptomic level, 935 DEGs could be identified
261 between the two bacteroid types (509 *A. afraspera* > *G. max* and 426 *G. max* > *A. afraspera*).
262 One notable feature of the transcriptome is the identification of four newly annotated ncRNA
263 and one new CDS amongst the 20 most induced DEGs in *A. afraspera* nodules and the presence
264 of five newly annotated CDS amongst the 20 most induced DEGs in *G. max* nodules (Table

265 S1). However, when considering only the functions that display congruent and significant
266 differences in terms of transcripts and protein levels between plant hosts, we fall down to 63
267 genes/proteins, 33 being induced in *A. afraspera* nodules and 30 being induced in *G. max*
268 nodules (Fig. 3B).

269 Interestingly, the phenylacetic acid degradation pathway (PaaABCDEIK, *blr2891*-*blr2897*)
270 was highly expressed in *A. afraspera* nodules (although only PaaABCD and PaaK have been
271 detected by proteomics), as well as a yet uncharacterized cluster of genes putatively involved
272 in toluene degradation (*blr3675*-*blr3680*). The chaperone GroEL2 is also specifically induced
273 in *A. afraspera*. Similarly, three S1 peptidases (Dop: *blr2591*, *blr3130* and *blr7274*) are highly
274 expressed in the nodules of this latter host together with a RND efflux pump (*bll3903*) and a
275 LTXQ motif protein (*bll6433*), a motif also found in the periplasmic stress response CpxP²⁶.
276 The over-accumulation of these proteins suggests that bacteroids are facing stressful conditions
277 during this interaction with *A. afraspera*. An uncharacterized ABC transporter solute binding
278 protein (*blr7922*) was also overexpressed in *A. afraspera*.

279 One αβ hydrolase (*blr6576*) and a TonB-dependent receptor-like protein (*bll2460*) were
280 over-accumulated in a *G. max*-specific manner. Similarly, an uncharacterized metabolic cluster
281 including transketolases (*blr2167*-*blr2170*), the heme biosynthetic enzyme HemN1 (*bll2007*)
282 and to a lesser extent an anthranilate phosphoribosyl-transferase (TrpD encoded by *bll2049*)
283 are overexpressed in soybean nodules.

284

285 **USDA110 transcriptomics data in the perspective of previously described regulons**
286 **and stimulons**

287 USDA110 is one of the best-characterized rhizobial strains in terms of transcriptomic
288 responses to various stimuli as well as the definition of regulons²⁷. We analyzed the behavior
289 of these previously defined gene networks in USDA110 in our dataset (Table S2). To initiate

290 the molecular dialog that leads to nodule formation, plants secrete flavonoids like genistein in
291 their root exudates, which are perceived by the rhizobia and trigger Nod factor production. At
292 14 dpi, when the nodule is formed and functioning, the genistein stimulon, which comprises the
293 NodD1, NodVW, TtsI and LafR regulons, is not anymore activated in bacteroids. The symbiotic
294 regulons controlled by NifA, FixK1, FixK2, FixLJ and sigma54 (RpoN) were activated *in*
295 *planta*, indicating that nitrogen fixation was going on in both hosts. Accordingly, the nitrogen
296 metabolism genes controlled by NtrC were activated *in planta*. Additionally, the PhyR/EcfG
297 regulon involved in general stress response is not activated in bacteroids. Differences between
298 hosts were however not observed for any of these regulons/stimulons. The only stimulon that
299 showed differential expression between hosts is the one involved in aromatic compound
300 degradation, which was highly expressed in *A. afraspera* nodules. Similar upregulation of the
301 vanillate degradation pathway was observed in the transcriptome of *Bradyrhizobium* sp.
302 ORS285 in *A. afraspera* and *A. indica* nodules¹⁷, suggesting that Dalbergioid hosts display a
303 higher aromatic compound content in nodules than *G. max*. In line with this hypothesis, some
304 of the most differentially accumulated sets of proteins (*A. afraspera* > *G. max*) are involved in
305 the degradation of phenylacetic acid (PaaABCDK and *bll0339*) suggesting that the bacterium
306 converts phenylalanine (or other aromatic compounds) ultimately to fumarate through this route
307 (Fig. 3B)²⁸. Similarly, enzymes of another pathway involved in phenolic compound degradation
308 (*blr3675-blr3680*) are accumulated in *A. afraspera* nodules (Fig. 3B, Table S1).

309

310 **Expression pattern of orthologous genes between ORS285 and USDA110 in *A.*
311 *afraspera* nodules**

312 In a previous study¹⁷, a transcriptome analysis was performed on *Bradyrhizobium* sp.
313 ORS285 in interaction with *A. afraspera* and in culture. *Bradyrhizobium* sp. ORS285 is a strain
314 that co-evolved with *A. afraspera*, leading to an efficient symbiosis hallmarked by TBD, *id est*

315 cell elongation and polyploidization of the bacteroids. In order to compare gene expression of
316 these two nodule-forming rhizobia in culture and *in planta*, we determined the set of
317 orthologous genes between the two strains using the Phyloprofile tool of Mage Microscope
318 website. This analysis yielded a total of 3725 genes (Table S3). The heatmap on Figure 4A
319 presents the modulation of gene expression (LFC) between *A. afraspera* nodules and the
320 bacterial culture for the orthologous genes in each bacterium, regardless of their statistical
321 significance. When taking FDR < 0.01 in account, we identified sets of genes that are
322 differentially expressed *in planta* in either bacterium or in both (Fig. 4B).

323 Only 343 genes displayed differential expression (FDR < 0.01 and |LFC| > 1.58) *in planta*
324 in both bacteria as compared to their respective culture control (Fig. 4C). A majority of these
325 genes (86.8%) exhibited congruent expression patterns. First, the *nif*, *fix* and *hup* genes are
326 commonly and highly induced in both strains during their symbiotic life with *A. afraspera*, a
327 hallmark of a functional symbiosis. However, there are differences in their expression level,
328 with a higher expression of the symbiotic genes in ORS285 (*nifHDK* represent 12.5% of all
329 reads in *A. afraspera* nodules)¹⁷ than in USDA110 (*nifHDK* represent only 2.5% of all reads in
330 *A. afraspera* nodules), consistently with a more efficient interaction occurring between ORS285
331 and *A. afraspera*. Additionally, the Kdp high affinity transport system, the phosphate (*pstCAB*,
332 *phoU*, *phoE*, *phoC*) and phosphonate metabolism (*phnHIJKL*) are activated *in planta* in both
333 bacteria (Fig. 4B-C). The stress-marker *dop* protease gene is also induced in both bacteria in *A.*
334 *afraspera* nodules (Fig. 4C).

335 Additionally, 1026 genes were differentially expressed solely in ORS285, and similarly
336 there was 604 DEG specific to USDA110 (Fig. 4B). For example, the general secretory pathway
337 seems to be specifically induced in ORS285¹⁷. Oppositely, USDA110 displays an induction of
338 the *rhcJQRU* genes which are involved in the injection of type three effector proteins that can
339 be important for the establishment of the symbiosis whereas they are not induced or even

340 repressed in ORS285 (Fig. 4B). This is also the case of the nitrite reductase encoding gene *nirK*
341 (*blr7089*/BRAD285_v2_0763; Fig. 4C). In addition, USDA110 induces the expression of an
342 ACC deaminase (*blr0241*), while its ortholog is repressed in ORS285 (BRAD285_v2_3570)
343 during symbiosis (Fig. 4C). Bacterial ACC deaminases can degrade ACC, a precursor of
344 ethylene, and thereby modulate ethylene levels in the plant host and promote the nodulation
345 process²⁹.

346

347 ***Bradyrhizobium diazoefficiens* USDA110 bacteroids undergo bona fide TBD in**
348 ***Aeschynomene afraspera* nodules despite very weak morphological and ploidy**
349 **modifications**

350 In a previous description of the *A. afraspera* - *B. diazoefficiens* USDA110 interaction, the
351 typical TBD features were not observed and the bacteroids were very similar to those in *G. max*
352 where no TBD occurs¹⁶. At the molecular level, accumulation of the replication initiation factor
353 DnaA is higher in soybean than in *A. afraspera* (Table S1). Similarly, the MurA peptidoglycan
354 synthesis enzyme (encoded by *bll0822*) that may play a role in cell elongation during TBD was
355 detected to similar levels in both bacteroids (Table S1). Taken together, the molecular data do
356 not clearly indicate whether USDA110 bacteroids undergo TBD in *A. afraspera*. Therefore, we
357 investigated the features of the USDA110 bacteroids in *A. afraspera* nodules in more detail.

358 We analyzed bacteroid differentiation features in USDA110 bacteroids extracted from
359 soybean and *A. afraspera* nodules. The interaction between *A. afraspera* and *Bradyrhizobium*
360 sp. ORS285 was used as a positive control for TBD features^{9,30,31}. TBD is characterized by cell
361 elongation. We quantified cell length, width, area and shape of purified bacteroids and culture
362 controls. Whereas ORS285 bacteroids were enlarged within *A. afraspera* nodules as compared
363 to their free-living counterparts, USDA110 bacteroids were similar to free-living bacteria in both
364 soybean and *A. afraspera* (Fig. 5A; Fig. S6). Another feature of TBD is endoreduplication.

365 Analysis of the bacterial DNA content of ORS285 bacteroids in *A. afraspera* by flow cytometry
366 shows peaks at 6C and more⁹. As expected, USDA110 bacteroids in *G. max* yields only two
367 peaks, at 1C and 2C, similarly to the cycling cells in the bacterial culture sample (Fig. 5B)¹⁶.
368 Strikingly, similar results were obtained for USDA110 in *A. afraspera*. Thus, with respect to
369 the DNA content and cell size, the USDA110 bacteroids do not display the typical TBD features
370 in *A. afraspera* nodules. Loss of membrane integrity is a third hallmark of TBD that likely
371 strongly contributes to the loss of viability of bacteroids. Time-course analysis of propidium
372 iodide (PI) uptake by bacteroids and the corresponding culture controls were performed to
373 assess bacteroid permeability (Fig. S7). Twenty minutes after PI application, USDA110
374 bacteroids from *A. afraspera* display an increased permeability that is much closer to ORS285
375 bacteroids in interaction with *A. afraspera* than to the low permeability of USDA110 bacteroids
376 from *G. max* nodules (Fig. 5C). Also the free-living counterparts exhibit a very low
377 permeability. Taken together, this suggests that the envelope of USDA110 bacteroids is more
378 permeable in the NCR-producing *A. afraspera* nodules, even if it does not reach the
379 permeability level of the ORS285 strain. To analyze bacterial viability, bacteroids extracted
380 from nodules were plated and the colony forming units (cfu) were determined (Fig. 5D). In *G.*
381 *max*, USDA110 formed 1.46×10^{10} colonies/mg nodule (~100% survival). Oppositely, ORS285
382 formed only 5.42×10^7 colonies/mg nodule in *A. afraspera* (~0.5% survival). Interestingly,
383 USDA110 formed 1.13×10^8 colonies/mg nodule in *A. afraspera* (~1% survival), indicating that,
384 despite the absence of cell enlargement and endoreduplication USDA110 bacteroids lose their
385 viability and undergo a *bona fide* terminal differentiation in *A. afraspera*. Thus, in the NCR-
386 producing plant *A. afraspera*, USDA110 bacteroids display a disconnection of the four
387 canonical TBD features (ie. cell size, ploidy level, membrane permeability and cell viability).
388

389 **Discussion**

390

391 ***Aeschynomene afraspera* triggers atypical but terminal differentiation of USDA110**
392 **bacteroids**

393 In a previous study, we noticed that, in *A. afraspera*, USDA110 forms a functional
394 symbiosis although bacteroids do not display features that are usually associated with TBD¹⁶.
395 Here we show that no endoreduplication and cell elongation of USDA110 occur in terminally
396 differentiated bacteroids that fix nitrogen in a suboptimal way. Accordingly, the protein level
397 of DnaA, the genome replication initiator, was higher in soybean than in *A. afraspera* bacteroids
398 and the MurA level was not different between bacteroid conditions, confirming that
399 polyploidization and cell elongation did not occur in this host. Such unusual terminal bacteroid
400 differentiation is reminiscent of the bacteroids in *Glycyrrhiza uralensis*. This plant of the IRLC
401 expresses NCR peptides¹¹. However, one of its compatible symbionts, *Sinorhizobium fredii*
402 strain HH103, does not undergo any loss of viability, no change in DNA content and no cell
403 elongation³², while another symbiont, *Mesorhizobium tianshanense* strain HAMBI 3372
404 showed all TBD features³³. The influence of the bacterial genotype on terminal/non-terminal
405 differentiation of bacteroids was also suggested in *Medicago truncatula* in which, the gene *hrrP*
406 might confer to some *Sinorhizobium* strains a resistance against the differentiation process
407 triggered by some *M. truncatula* ecotypes³⁴. In these two IRLC plants (ie. *M. truncatula* and *G.*
408 *uralensis*), bacteria undergo a complete TBD or no TBD at all in a strain-dependent manner,
409 but there is no clear uncoupling of the features of TBD (cell
410 elongation/endoreduplication/ altered viability) as shown here in the case of *B. diazoefficiens*
411 USDA110-*A. afraspera*.

412 The surprising differentiation of USDA110 in *A. afraspera* nodules raises questions about
413 the molecular mechanisms supporting this phenomenon. We consider two possible hypotheses:
414 strain USDA110 might be more sensitive to the differentiation factors of the host than strain

415 ORS285 and be rapidly “terminally” differentiated, before the other differentiation features,
416 that are potentially important for symbiotic efficiency, can take place. Alternatively, USDA110
417 might be resistant to the plant effectors that trigger the elongation and polyploidization features.

418 In agreement with the latter possibility, the application of NCR peptides has very limited
419 effect on strain USDA110 as compared to *S. meliloti* and to other plant-associated bacteria^{16,35}.
420 NCR insensitivity may be due to the thick hopanoid layer that is present in the outer membrane
421 of strain USDA110, as the hopanoid biosynthesis mutant *hpnH* is more sensitive to NCR
422 peptides and shows symbiotic defects in *A. afraspera* but not in *G. max*³⁶. Moreover, the altered
423 peptidoglycan structure in the strain USDA110 DD-carboxypeptidase mutant resulted in an
424 increased TBD process with endoreduplicated and elongated bacteroids in *A. afraspera*¹⁶. This
425 suggests that the envelope of strain USDA110 prevents a canonical TBD to occur. Possibly,
426 NCR peptides are not able to reach their intracellular targets required to induce
427 endoreduplication and cell division arrest, while their effect on cell viability through pore
428 formation and membrane destabilization is still effective.

429 A survey of TBD in the legumes has identified multiple occurrences of the process in several
430 subclades of the legumes but found that the majority of legumes do not have TBD³⁷. The
431 classification in this study was based on a morphological analysis of the bacteroids. Ancestral
432 state reconstruction based on this classification suggested that the non-differentiated bacteroids
433 are ancestral and that TBD evolved at least five times independently in legumes³⁷. The
434 discovery of bacteroids that are terminally differentiated without any obvious morphological
435 changes opens the possibility that the occurrence of TBD might be underestimated in the
436 legume family. Similarly, in the IRLC clade, the extent of morphological bacteroid
437 differentiation was correlated to the size of the cationic NCR peptides repertoire and in legumes
438 with few NCR peptides, the morphological modification of bacteroids can be minor^{11,33}. In
439 addition, at the molecular level, TBD is originally ascribed to the production of symbiotic

440 antimicrobial peptides, the NCRs, by nodules⁷, but more recently, other types of antimicrobial
441 peptides such as the NCR-like, GRP, MBP1 and CAPE peptides specifically produced in
442 nodules of different plants were proposed to contribute to bacteroid differentiation^{9,38-40}. Thus,
443 if TBD would indeed be more widespread than currently estimated on the basis of
444 morphological bacteroid features, the currently proposed evolutionary scenario of bacteroid
445 formation might require revision.

446

447 **Terminal differentiation is associated with specific stress response**

448 The TBD of strain USDA110 in *A. afraspera* is associated with a higher accumulation of
449 stress markers compared to the *G. max* bacteroids. These markers include four proteases (Dop,
450 Lon_2, *blr3130* and *blr7274*) and one chaperonin (GroEL_2). Similar induction of proteases
451 and chaperonins have been reported in NCR-treated *S. meliloti* cultures³⁵, indicating that this
452 response may be linked to the perception of *A. afraspera* NCR-like peptides in USDA110.

453 The genes encoding these stress related proteins are not part of the well-characterized
454 general stress response (GSR) controlled by the PhyR/EcfG signaling cascade in *B.*
455 *diazoefficiens* USDA110⁴¹. On the other hand, we found that the PhyR/EcfG regulon in
456 USDA110 is not activated in the bacteroids of both host plants (Table S2). This observation
457 contrasts with our previous study of *Bradyrhizobium* sp. ORS285 transcriptome during
458 symbiosis with *Aeschynomene* plants, which showed that the PhyR/EcfG cascade was
459 upregulated *in planta*¹⁷. Nevertheless, the expression of the Dop protease was induced in *A.*
460 *afraspera* in both bacteria (Fig. 4C). Together, the omics data suggest that bacteroids of
461 *Bradyrhizobium* spp. activate stress-related genes in the TBD-inducing *A. afraspera* host but
462 differences exist in the activation of specific stress responses at the strain level.

463

464 **Correlation between bacteroid differentiation features and symbiotic efficiency for the**
465 **plant**

466 TBD is associated with the massive production of symbiotic antimicrobial peptides such as
467 NCR, NCR-like and CAPE peptides in different plants^{5,9,38,40}. They represent ~10% of the
468 nodule transcriptomes in *M. truncatula* (analysis of the data from ref 42) and their production
469 is thus potentially a strong energetic cost for the plant, raising questions about the benefits of
470 the TBD process. TBD appeared independently in different legume clades^{9,37}, suggesting that
471 plants imposing this process obtain an advantage which might be a higher symbiotic benefit.
472 Increased symbiotic efficiency has indeed been observed in hosts imposing TBD^{17,43,44}. The
473 findings reported here, comparing bacteroids and symbiotic efficiency in *A. afraspera* infected
474 with strain ORS285 and strain USDA110, are in agreement with this hypothesis. Also in the
475 symbiosis of *M. truncatula* in interaction with different *S. meliloti* strains, a similar correlation
476 was observed between the level of bacteroid differentiation and the plant growth stimulation⁴⁵.
477 However, the simultaneous analysis of the bacteroid differentiation and symbiotic performance
478 of an extended set of *Aeschynomene-Bradyrhizobium* interactions has shown that, perhaps not
479 unexpectedly, the symbiotic efficiency of the plant-bacterium couple is not solely correlated
480 with bacteroid differentiation and that other factors can interfere with the symbiotic efficiency
481 as well⁴⁶.

482

483 **Conclusion**

484 *Bradyrhizobium diazoefficiens* USDA110 is a major model in the legume-rhizobium
485 symbiosis, mainly thanks to its interaction with *G. max*, the worldwide most cultivated legume.
486 Although omic studies have been conducted in this strain in symbiosis with various hosts^{13,25},
487 this is the first time that this bacterium is studied at the molecular level in symbiosis with a
488 NCR-producing plant that normally trigger a typical terminal bacteroid differentiation in its

489 symbionts. The symbiosis between USDA110 and *A. afraspera* is functional even if nitrogen
490 fixation and plant benefits are sub-optimal.

491 Terminal bacteroid differentiation is taking place in the NCR-producing host *A. afraspera*,
492 as bacterial viability is impaired in USDA110 bacteroids, whereas morphological changes and
493 the cell cycle switch to endoreduplication are not observed. We also show by combining
494 proteomics and transcriptomics that the bacterial symbiotic program is expressed in *A.*
495 *afraspera* nodules in a similar way as in *G. max*, although host-specific patterns were also
496 identified. However, the bacterium is under stressful conditions in the *A. afraspera* host,
497 possibly due to the production of NCR-like peptides in this plant. Integration of datasets from
498 different bacteria in symbiosis with a single host, like ORS285 and USDA110 in symbiosis
499 with *A. afraspera*, shed light on the differences in the stress responses activated in *A. afraspera*
500 and confirmed that the symbiosis is functional but suboptimal in this interaction. The molecular
501 data presented here provide a set of candidate functions that could be analyzed for their
502 involvement in the adaptation to a new host and to the TBD process.

503 **Material and Methods**

504 **Bacterial cultures and bacteroid extraction**

505 *B. diazoefficiens* USDA110⁴⁷ and *Bradyrhizobium* sp. ORS285 were cultivated in YM
506 medium at 30°C in a rotary shaker⁴⁸. For transcriptomic analysis, culture samples (OD_{600nm} =
507 0.5) were collected and treated as in Chapelle et al. (2015)⁴⁹.

508 *G. max* ecotype Williams 82 and *A. afraspera* seeds were surface-sterilized and the plants
509 were cultivated and infected with rhizobia for nodule formation as described in Barrière et al.
510 (2017)¹⁶. Nodules were collected at 14 days post inoculation (dpi), immediately immersed in
511 liquid nitrogen and stored at -80°C until use. Each tested condition (in culture and *in planta*)
512 was produced in biological triplicates.

513

514 **Phylogeny analysis**

515 Nucleotide sequence of *matK* genes were collected on NCBI using accession numbers
516 described in references 50 and 51 and analyzed on phylogeny.fr (www.phylogeny.fr). They
517 were aligned using ClustalW with manual corrections, before running a phyML (GTR - Gamma
518 model) analysis with 500 bootstraps. A Bayesian inference tree was also generated (GTR + G
519 + I) and provided similar topology as the maximum likelihood tree (data not shown). Trees
520 were visualized and customized using TreeDyn.

521

522 **Genome annotation and RNA-seq analysis**

523 Nodule and bacterial culture total RNA was extracted and treated as previously described
524 in ¹⁷. Oriented (strand-specific) libraries were produced using the SOLiD Total RNA-seq kit
525 (Life Technologies) and were sequenced on a SOLiD 3 station yielding ~40 million 50bp single
526 reads. Trimming and normalization of the reads were performed using the CLC workbench
527 software. Subsequently, the reads were used to annotate the genome using EugenePP²³, and the
528 mapping was performed using this new genome annotation. Analysis of the transcriptome using
529 DE-seq2 and data representation were performed as previously described¹⁷. Differentially
530 expressed genes (DEG) showed an absolute log₂ fold change (|LFC|) > 1.58 (ie. fold change >
531 3) with a false discovery rate (FDR) < 0.01.

532

533 **Proteomic analysis**

534 Bacteroids were extracted from 14 dpi frozen nodules⁶, while bacterial culture samples were
535 collected as above, and the bacterial pellets were resuspended in -20°C acetone and lysed by
536 sonication. Protein solubilization, dosage, digestion (trypsin 2% w/w) and solid phase
537 extraction (using Phenomenex polymeric C18 column) were performed as described before⁵².
538 Peptides from 800 ng of proteins were analyzed by LC-MS/MS with a Q Exactive mass

539 spectrometer (Thermo Electron) coupled to a nanoLC Ultra 2D (Eksigent) using a
540 nanoelectrospray interface (non-coated capillary probe, 10 μ i.d.; New Objective). Peptides
541 were loaded on a Biosphere C18 trap-column (particle size: 5 μ m, pore size: 12 nm, inner/outer
542 diameters: 360/100 μ m, length: 20 mm; NanoSeparations) and rinsed for 3 min at 7,5 μ l minute
543 of 2% Acetonitrile (ACN), 0,1% Formic acid (FA) in water. Peptides were then separated on a
544 Biosphere C18 column (particle size: 3 μ m, pore size: 12 nm, inner/outer diameters: 360/75
545 μ m, length: 300 mm; NanoSeparations) with a linear gradient from 5% of 0,1% FA in ACN
546 (buffer B) and 95% of 0,1% FA in Water (buffer A) to 35% of buffer B and 65% of buffer A
547 in 80 min at 300nl/min followed by a rinsing step at 95% of buffer B and 5% of buffer A for 6
548 min and a regeneration step with parameters of the start of the gradient for 8 min. peptide ions
549 were analyzed using Xcalibur 2.1 software in data dependent mode with the following
550 parameters: (I) full ms was acquire for the 400-1400 mz range at a resolution of 70000 with an
551 AGC target of 3.10⁶; (ii) MS² scan was acquired at a resolution of 17500 with an agc target of
552 5.10⁴, a maximum injection time of 120 ms and an isolation window of 3 m/z. The normalized
553 collision energy was set to 27. MS² scan was performed for the eight most intense ions in
554 previous full MS scan with an intensity threshold of 1.10³ and a charge between 2 and 4.
555 Dynamic exclusion was set to 50s. After conversion to mzXML format using msconvert
556 (3.0.3706)⁵³, data were searched using X!tandem (version 2015.04.01.1)⁵⁴ against the
557 USDA110 reannotated protein database and a homemade database containing current
558 contaminants. In a first pass trypsin was set to strict mode and cysteine carbamidomethylation
559 as a fixed modification and methionine oxidation, protein N-terminal acetylation with or
560 without protein N-terminal methionine excision, N-terminal glutamine and
561 carbamidomethylated cysteine deamidation, N-terminal glutamic dehydration as potential
562 modifications. In a refine pass, Semi enzymatic peptides were allowed. Proteins inference was
563 performed using X!TandemPipeline (version 3,4,3)⁵⁵. A protein was validated with an E-value

564 < 10⁻⁵ and 2 different peptides with an E-value < 0.05. Protein from contaminant database
565 (*Glycine max* proteins and unpublished *Aeschynomene* Expressed Sequence Tags) were
566 removed after inference. Proteins were quantified using the spectral counting method⁵⁶. To
567 discriminate differentially accumulated proteins (DAPs), ANOVA analysis was performed on
568 the spectral counts and proteins were considered DAP when p-value < 0.05.

569

570 **Metabolomic analysis**

571 Metabolites and cofactors were extracted from lyophilized nodules and analyzed by GC-
572 MS and LC-MS respectively according to Su et al. (2016)⁵⁷.

573

574 **Plant biomass and nitrogen fixation analysis**

575 Dry mass of shoot, root and nodules was measured, and shoot-root mass ratio was
576 calculated. The mass gain per g of dry nodule was calculated as the difference between total
577 mean masses of the plants of interest and of the non-inoculated plants, divided by the mean
578 mass of nodules. Thirty plants were used per condition. Nitrogenase activity was assessed by
579 Acetylene Reduction Assay (ARA) on ten plants per condition as previously described³¹. The
580 elemental analysis of leaf carbon and nitrogen content was performed as described in reference
581 18.

582

583 **Analysis of *B. diazoefficiens* USDA110 regulons and stimulons**

584 Gene sets defined as regulons and stimulons were collected from the literature and the
585 regulons/stimulons were considered as activated/repressed when ≥ 40% of the corresponding
586 genes were DEG in a host plant as compared to the culture condition.

587

588 **Comparison of orthologous gene expression between *B. diazoefficiens* USDA110 and** 589 ***Bradyrhizobium* sp. ORS285**

590 The list of orthologous genes between USDA110 and ORS285 was determined using the
591 Phyloprofile tool of the MicroScope-MAGE platform⁵⁸, with identity threshold of 60%,
592 maxLrap > 0 and minLrap > 0.8. The RNA-seq data from reference 17 and those of this study
593 were used to produce heatmaps, for the genes displaying FDR < 0.01 (*A. afraspera* vs. YM),
594 using R (v3.6.3) and drawn using pheatmap (v1.0.12) coupled with kohonen (v3.0.10) for gene
595 clustering using the Self Organizing Maps (SOM) method. The DEG in both organisms (*A.*
596 *afraspera* vs YM) were plotted for USDA110 and ORS285.

597

598 **Analysis of TBD features**

599 Bacteroids were extracted from 14 dpi nodules and analyzed using a CytoFLEX S
600 (Beckman-Coulter)³¹. For ploidy and live/dead analyses, samples were stained with propidium
601 iodide (PI, ThermoFisher, 50 $\mu\text{g.mL}^{-1}$ final) and Syto9 (ThermoFisher, 1.67 μM final). PI
602 permeability was assessed over time on live bacteria. *Bradyrhizobium* sp. ORS285.pMG103-
603 *nptII-GFP*³⁰ and *B. diazoefficiens* USDA110 sYFP2-1⁵⁹ strains were used to distinguish
604 bacteroid from debris during flow cytometry analysis. For each time point, the suspension was
605 diluted 50 times for measurement in the flow-cytometer. The percentage of bacteroids
606 permeable to PI was estimated as the ratio of PI-positive over total bacteroids (GFP/YFP
607 positive). Heat-killed bacteroids were used as positive control to identify the PI-stained
608 bacteroid population.

609 For bacteroid viability assays, nodules were collected and surface sterilized (1 min NaClO
610 0.4%, 1 min 70% ethanol, two washes in sterile water). Bacteroids were subsequently prepared
611 as previously described³¹ and serially diluted and plated (five μl per spot) in triplicate on YM
612 medium containing 50 $\mu\text{g.mL}^{-1}$ carbenicillin. Colony-forming units (cfu) were counted five
613 days post plating and divided by the total nodule mass.

614 Bacterial cell shape, length and width were determined using confocal microscopy image
615 analysis. Bacteroid extracts and stationary phase bacteria cultures were stained with 2.5 nM Syto9
616 for 10 minutes at 37°C and mounted between slide and coverslip. Bacteria imaging was
617 performed on a SP8 laser scanning confocal microscope (Leica Microsystems) equipped with
618 hybrid detectors and a 63x oil immersion objective (Plan Apo, NA: 1.4, Leica). For each
619 condition, multiple z-stacks (2.7µm width, 0.7 µm step) were automatically acquired
620 (excitation: 488 nm; collection of fluorescence: 520-580 nm).

621 Prior to image processing, each stack was transformed as a maximum intensity projection
622 using ImageJ software (<https://imagej.nih.gov/ij/>). Bacteria detection was performed with
623 MicrobeJ (<https://www.microbej.com/>)⁶⁰. First, bacteria were automatically detected on every
624 image using an intensity based thresholding method with a combination of morphological filters
625 (area: 1-20 µm²; length: 1 µm-∞; width: 0.5-1.3 µm) and every object was fitted with a “Rod-
626 shaped” bacteria model. To ensure high data quality every image was manually checked to
627 remove false positive (mainly plant residues) and include rejected objects (mainly fused
628 bacteria). Then the morphology measurements and figures were directly extracted from
629 MicrobeJ. ORS285 in culture and in symbiosis with *A. afraspera* were used as references for
630 the analysis of TBD features.

631

632 **Western blot analysis**

633 Detection of NifH by western blotting was performed using a commercial polyclonal
634 antibody against a NifH peptide (Agrisera) respectively. The western blotting was carried out
635 as previously described⁶¹ using bacterial exponential (OD_{600nm} = 0.5) and stationary (OD_{600nm} >
636 2.5) phase cultures as well as 14 dpi nodule-extracted bacteroids.

637

638 **Acknowledgments**

639 The authors would like to thank Dora Latinovics for production and sequencing of the RNA-
640 seq libraries and Mélisande Blein-Nicolas for her advices regarding the statistical analysis of
641 the proteomic dataset. Q.N. and F.L. were supported by a PhD fellowship from the Université
642 Paris-Sud. The present work has benefited from the core facilities of Imagerie-Gif
643 (<http://www.i2bc.paris-saclay.fr>), member of IBiSA (<http://www.ibisa.net>), supported by
644 ‘France-BioImaging’ (ANR-10-INBS-04-01), and the Labex ‘Saclay Plant Sciences’ (ANR-
645 11-IDEX-0003-02). This work was funded by the Agence Nationale de la Recherche, grants n°
646 ANR-13-BSV7-0013 and ANR-17-CE20-0011 and used resources from the National Office for
647 Research, Development and Innovation of Hungary, grant n° 120120 to A.K.

648

649 **Authors' contribution**

650 QN, FL, PM, BGo and BA designed the work. QN, FL, AC, TB, MB, FGu, ES, ST and OP
651 performed the experiments. QN, FL, MB, ES, YD, BGa, FGi, IN, AK, MZ, PM, BGo and BA
652 analyzed the data. QN, FL, PM, BGo and BA wrote the paper.

653

654 **References**

- 655 1. Erisman, J.W., Galloway, J.N., Seitzinger, S., Bleeker, A., Dise, N.B., Petrescu,
656 A.M.R., et al. (2013) Consequences of human modification of the global nitrogen cycle.
657 *Philos Trans R Soc B Biol Sci* **368**: 20130116–20130116.
- 658 2. Zhao, C., Liu, B., Piao, S., Wang, X., Lobell, D.B., Huang, Y., et al. (2017) Temperature
659 increase reduces global yields of major crops in four independent estimates. *Proc Natl
660 Acad Sci U S A* **114**: 9326–9331.
- 661 3. Oldroyd, G. (2013) Speak, friend, and enter: signalling systems that promote beneficial
662 symbiotic associations in plants. *Nat Rev Microbiol* **11**: 252–263.

663 4. Gourion, B. and Alunni, B. (2018) Strain-specific symbiotic genes: A new level of
664 control in the intracellular accommodation of rhizobia within legume nodule cells. *Mol
665 Plant-Microbe Interact* **31**: 287–288.

666 5. Mergaert, P., Nikovics, K., Kelemen, Z., Maunoury, N., Vaubert, D., Kondorosi, A., et
667 al. (2003) A novel family in *Medicago truncatula* consisting of more than 300 nodule-
668 specific genes coding for small, secreted polypeptides with conserved cysteine motifs.
669 *Plant Physiol* **132**: 161–73.

670 6. Mergaert, P., Uchiumi, T., Alunni, B., Evanno, G., Cheron, A., Catrice, O., et al. (2006)
671 Eukaryotic control on bacterial cell cycle and differentiation in the rhizobium-legume
672 symbiosis. *Proc Natl Acad Sci U S A* **103**: 5230–5235.

673 7. Van de Velde, W., Zehirov, G., Szatmari, A., Debreczeny, M., Ishihara, H., Kevei, Z.,
674 et al. (2010) Plant peptides govern terminal differentiation of bacteria in symbiosis.
675 *Science* **327**: 1122–1126.

676 8. Guefrachi, I., Nagymihaly, M., Pislariu, C.I., Van de Velde, W., Ratet, P., Mars, M., et
677 al. (2014) Extreme specificity of NCR gene expression in *Medicago truncatula*. *BMC
678 Genomics* **15**(1):712.

679 9. Czernic, P., Gully, D., Cartieaux, F., Moulin, L., Guefrachi, I., Patrel, D., et al. (2015)
680 Convergent evolution of rhizosymbiont differentiation in Dalbergioid and Inverted
681 Repeat-Lacking Clade legumes mediated by nodule-specific cysteine-rich peptides.
682 *Plant Physiol* **169**: 1254–1265.

683 10. Alunni, B., and Gourion, B. (2016) Terminal bacteroid differentiation in the legume-
684 rhizobium symbiosis: nodule-specific cysteine-rich peptides and beyond. *New Phytol*
685 **211**: 411–417.

686 11. Montiel, J., Downie, J.A., Farkas, A., Bihari, P., Herczeg, R., Bálint, B., et al. (2017)
687 Morphotype of bacteroids in different legumes correlates with the number and type of
688 symbiotic NCR peptides. *Proc Natl Acad Sci U S A* **114**: 5041–5046.

689 12. Farkas, A., Maróti, G., Dürgo, H., Györgypal, Z., Lima, R.M., Folkl-Medzihradsky, K.,
690 Kereszt, A., Mergaert, P., and Kondorosi, E. (2014) *Medicago truncatula* symbiotic
691 peptide NCR247 contributes to bacteroid differentiation through multiple mechanisms.
692 *Proc Natl Acad Sci U S A* **111**: 5183–5188.

693 13. Koch, M., Delmotte, N., Rehrauer, H., Vorholt, J.A., Pessi, G., and Hennecke, H. (2010)
694 Rhizobial adaptation to hosts, a new facet in the legume root-nodule symbiosis. *Mol
695 Plant-Microbe Interact* **23**: 784–790.

696 14. Renier, A., Maillet, F., Fardoux, J., Poinsot, V., Giraud, E., and Nouwen, N. (2011)
697 Photosynthetic *Bradyrhizobium* Sp. strain ORS285 synthesizes 2-O-methylfucosylated
698 lipochitooligosaccharides for nod gene-dependent interaction with *Aeschynomene*
699 plants. *Mol Plant Microbe Interact* **24**: 1440–7.

700 15. Ledermann, R., Bartsch, I., Müller, B., Wülsner, J., and Fischer, H.M. (2018) A
701 functional general stress response of *Bradyrhizobium diazoefficiens* is required for early
702 stages of host plant infection. *Mol Plant-Microbe Interact* **31**: 537–547.

703 16. Barrière, Q., Guefrachi, I., Gully, D., Lamouche, F., Pierre, O., Fardoux, J., et al. (2017)
704 Integrated roles of BclA and DD-carboxypeptidase 1 in *Bradyrhizobium* differentiation
705 within NCR-producing and NCR-lacking root nodules. *Sci Rep* **7**: 1–13.

706 17. Lamouche, F., Gully, D., Chaumeret, A., Nouwen, N., Verly, C., Pierre, O., et al. (2019)
707 Transcriptomic dissection of *Bradyrhizobium* sp. strain ORS285 in symbiosis with
708 *Aeschynomene* spp. inducing different bacteroid morphotypes with contrasted symbiotic
709 efficiency. *Environ Microbiol.* **21**: 3244–3258.

710 18. Lamouche, F., Chaumeret, A., Guefrachi, I., Barrière, Q., Pierre, O., Guérard, F., et al.
711 (2019) From intracellular bacteria to differentiated bacteroids: transcriptome and
712 metabolome analysis in *Aeschynomene* nodules using the *Bradyrhizobium* sp. ORS285
713 *bclA* mutant. *J. Bacteriol.* **201**: e00191-19.

714 19. Andrews, M., Raven, J.A., Lea, P.J., and Sprent, J.I. (2006) A role for shoot protein in
715 shoot-root dry matter allocation in higher plants. *Ann Bot* **97**: 3-10.

716 20. Collier, R., and Tegeder, M. (2012) Soybean ureide transporters play a critical role in
717 nodule development, function and nitrogen export. *Plant J.* **72**: 355-67.

718 21. Ross, E.J.H.H., Kramer, S.B., and Dalton, D.A. (1999) Effectiveness of ascorbate and
719 ascorbate peroxidase in promoting nitrogen fixation in model systems. *Phytochemistry*
720 **52**: 1203–1210.

721 22. Bashor, C.J. and Dalton, D.A. (1999) Effects of exogenous application and stem
722 infusion of ascorbate on soybean (*Glycine max*) root nodules. *New Phytol* **142**: 19–26.

723 23. Sallet, E., Gouzy, J., and Schiex, T. (2014) EuGene-PP: a next-generation automated
724 annotation pipeline for prokaryotic genomes. *Bioinformatics* **30**: 2659–61.

725 24. Bittner, A.N., Foltz, A., and Oke, V. (2007) Only one of five *groEL* genes is required
726 for viability and successful symbiosis in *Sinorhizobium meliloti*. *J Bacteriol* **189**: 1884–
727 9.

728 25. Lardi, M., Murset, V., Fischer, H. M., Mesa, S., Ahrens, C. H., Zamboni, N. et al. (2016)
729 Metabolomic Profiling of *Bradyrhizobium diazoefficiens*-Induced Root Nodules
730 Reveals Both Host Plant-Specific and Developmental Signatures. *Int J Mol Sci* **17**(6) :
731 815.

732 26. Thede, G. L., Arthur, D. C., Edwards, R. A., Buelow, D. R., Wong, J. L., Raivio, T. L.,
733 & Glover, J. N. (2011) Structure of the periplasmic stress response protein CpxP.
734 *Journal Bacteriol* **193**(9): 2149–57.

735 27. diCenzo, G.C., Zamani, M., Checcucci, A., Fondi, M., Griffitts, J.S., Finan, T.M., and
736 Mengoni, A. (2018) Multi-disciplinary approaches for studying rhizobium – legume
737 symbioses. *Peer J* cjm-2018-0377.

738 28. Teufel, R., Mascaraque, V., Ismail, W., Voss, M., Perera, J., Eisenreich, W., et al. (2010)
739 Bacterial phenylalanine and phenylacetate catabolic pathway revealed. *Proc Natl Acad
740 Sci U S A* **107**: 14390–5.

741 29. Okazaki, S., Nukui, N., Sugawara, M., and Minamisawa, K. (2004) Rhizobial strategies
742 to enhance symbiotic interactions: rhizobitoxine and 1-aminocyclopropane-1-
743 carboxylate deaminase. *Microb. Environ* **19**: 99–111.

744 30. Bonaldi, K., Gargani, D., Prin, Y., Fardoux, J., Gully, D., Nouwen, N., et al. (2011)
745 Nodulation of *Aeschynomene afraspera* and *A. indica* by photosynthetic
746 *Bradyrhizobium* sp. strain ORS285: the Nod-dependent versus the Nod-independent
747 symbiotic interaction. *Mol Plant-Microbe Interact* **24**: 1359–1371.

748 31. Guefrachi, I., Pierre, O., Timchenko, T., Alunni, B., Barrière, Q., Czernic, P., et al.
749 (2015) *Bradyrhizobium* BclA is a peptide transporter required for bacterial
750 differentiation in symbiosis with *Aeschynomene* legumes. *Mol Plant-Microbe Interact*
751 **28**: 1155–1166.

752 32. Crespo-Rivas, J.C., Guefrachi, I., Mok, K.C., Villaécija-Aguilar, J.A., Acosta-Jurado,
753 S., Pierre, O., et al. (2016) *Sinorhizobium fredii* HH103 bacteroids are not terminally
754 differentiated and show altered O-antigen in nodules of the Inverted Repeat-Lacking
755 Clade legume *Glycyrrhiza uralensis*. *Environ Microbiol* **18**: 2392–2404.

756 33. Montiel, J., Szűcs, A., Boboescu, I.Z., Gherman, V.D., Kondorosi, E., and Kereszt, A.
757 (2016) Terminal bacteroid differentiation is associated with variable morphological
758 changes in legume species belonging to the Inverted Repeat-Lacking Clade. *Mol Plant
759 Microbe Interact* **29**(3): 210-9.

760 34. Price, P.A., Tanner, H.R., Dillon, B.A., Shabab, M., Walker, G.C., and Griffitts, J.S.
761 (2015) Rhizobial peptidase HrrP cleaves host-encoded signaling peptides and mediates
762 symbiotic compatibility. *Proc Natl Acad Sci U S A* **112**: 15244–15249.

763 35. Tirim, H., Szücs, A., Farkas, A., Pap, B., Lima, R.M., Maróti, G., et al. (2013)
764 Antimicrobial nodule-specific cysteine-rich peptides induce membrane depolarization-
765 associated changes in the transcriptome of *Sinorhizobium meliloti*. *Appl Environ
766 Microbiol* **79**: 6737–6746.

767 36. Kulkarni, G., Busset, N., Molinaro, A., Gargani, D., Chaintreuil, C., Silipo, A., et al.
768 (2015) Specific hopanoid classes differentially affect free-living and symbiotic states of
769 *Bradyrhizobium diazoefficiens*. *MBio* **6**: 1–9.

770 37. Oono, R., Schmitt, I., Sprent, J.I., and Denison, R.F. (2010) Multiple evolutionary
771 origins of legume traits leading to extreme rhizobial differentiation. *New Phytol* **187**(2):
772 508-20

773 38. Karmakar, K., Kundu, A., Rizvi, A.Z., Dubois, E., Severac, D., Czernic, P., et al. (2019)
774 Transcriptomic analysis with the progress of symbiosis in ‘crack-entry’ legume *Arachis
775 hypogaea* highlights its contrast with ‘infection thread’ adapted legumes. *Mol Plant-
776 Microbe Interact* **32**(3):271-285.

777 39. Kereszt, A., Mergaert, P., Montiel, J., Endre, G., and Kondorosi, E. (2018) Impact of
778 plant peptides on symbiotic nodule development and functioning. *Front Plant Sci.*
779 **9**:1026

780 40. Trujillo, D.I., Silverstein, K.A.T., and Young, N.D. (2019) Nodule-specific PLAT
781 domain proteins are expanded in the *Medicago* lineage and required for nodulation. *New
782 Phytol* **222**: 1538–1550.

783 41. Gourion, B., Sulser, S., Frunzke, J., Francez-Charlot, A., Stiefel, P., Pessi, G., et al.
784 (2009) The PhyR- σ EcfG signalling cascade is involved in stress response and symbiotic
785 efficiency in *Bradyrhizobium japonicum*. *Mol Microbiol* **73**: 291–305.

786 42. Roux, B., Rodde, N., Jardinaud, M.F., Timmers, T., Sauviac, L., Cottret, L., et al. (2014)
787 An integrated analysis of plant and bacterial gene expression in symbiotic root nodules
788 using laser-capture microdissection coupled to RNA sequencing. *Plant J* **77**(6):817-37.

789 43. Sen, D. and Weaver, R.W. (1981) A comparison of nitrogen-fixing ability of peanut,
790 cowpea and siratro plants nodulated by different strains of *Rhizobium*. *Plant Soil* **60**:
791 317–319.

792 44. Oono, R. and Denison, R.F. (2010) Comparing symbiotic efficiency between swollen
793 versus nonswollen rhizobial bacteroids. *Plant Physiol* **154**: 1541–1548.

794 45. Kazmierczak, T., Nagymihaly, M., Lamouche, F., Barriere, Q., Guefrachi, I., Alunni,
795 B., et al. (2017) Specific host-responsive associations between *Medicago truncatula*
796 accessions and *Sinorhizobium* strains. *Mol. Plant Microbe Interact.* **30**:399–409.

797 46. Lamouche, F., Bonadé-Bottino, N., Mergaert, P., and Alunni, B. (2019) Symbiotic
798 efficiency of spherical and elongated bacteroids in the *Aeschynomene-Bradyrhizobium*
799 symbiosis. *Front. Plant Sci* **10**: 377.

800 47. Regensburger, B. and Hennecke, H. (1983) RNA polymerase from *Rhizobium*
801 *japonicum*. *Arch Microbiol* **135**: 103–109.

802 48. Giraud, E., Hannibal, L., Fardoux, J., Verméglia, A., and Dreyfus, B. (2000) Effect of
803 *Bradyrhizobium* photosynthesis on stem nodulation of *Aeschynomene sensitiva*. *Proc
804 Natl Acad Sci U S A* **97**: 14795–14800.

805 49. Chapelle, E., Alunni B, Malfatti P, Solier L, Pedron J, Kraepiel Y, Van Gijsegem F.
806 (2015) A straightforward and reliable method for bacterial *in planta* transcriptomics:

807 application to the *Dickeya dadantii/Arabidopsis thaliana* pathosystem. *Plant J* **82**:352–
808 362.

809 50. Azani, N., Babineau, M., Bailey, C.D., Banks, H., Barbosa, A.R., Pinto, R.B., *et al.*
810 (2017) A new subfamily classification of the Leguminosae based on a taxonomically
811 comprehensive phylogeny – The Legume Phylogeny Working Group (LPWG). *Taxon*
812 **66**: 44–77.

813 51. Brottier, L., Chaintreuil, C., Simion, P., Scornavacca, C., Rivallan, R., Mournet, P., *et*
814 *al.* (2018) A phylogenetic framework of the legume genus *Aeschynomene* for
815 comparative genetic analysis of the Nod-dependent and Nod-independent symbioses.
816 *BMC Plant Biol* **18**: 333.

817 52. Langella O, Valot B, Jacob D, Balliau T, Flores R, Hoogland C, Joets J, Zivy M. (2013)
818 Management and dissemination of MS proteomic data with PROTEICdb: example of a
819 quantitative comparison between methods of protein extraction. *Proteomics*
820 13(9):1457-66.

821 53. Kessner D, Chambers M, Burke R, Agus D, Mallick P. (2008) ProteoWizard: open
822 source software for rapid proteomics tools development. *Bioinformatics* **24**(21):2534-6.

823 54. Craig R, Beavis RC. (2004) TANDEM: matching proteins with tandem mass spectra.
824 *Bioinformatics* **20**(9):1466-7.

825 55. Langella O, Valot B, Balliau T, Blein-Nicolas M, Bonhomme L, Zivy M. (2017)
826 X!TandemPipeline: A tool to manage sequence redundancy for protein inference and
827 phosphosite identification. *J Proteome Res.* **16**(2):494-503.

828 56. Delmotte N, Mondy S, Alunni B, Fardoux J, Chaintreuil C, Vorholt JA, Giraud E,
829 Gourion B. (2014) *Int J Mol Sci.* **15**(3):3660-70.

830 57. Su, F., Gilard, F., Guérard, F., Citerne, S., Clément, C., Vaillant-Gaveau, N., and
831 Dhondt-Cordelier, S. (2016) Spatio-temporal responses of *Arabidopsis* leaves in

832 photosynthetic performance and metabolite contents to *Burkholderia phytofirmans*
833 PsJN. *Front Plant Sci* **7**: 1–15.

834 58. Médigue, C., Calteau, A., Cruveiller, S., Gachet, M., Gautreau, G., Josso, A., *et al.*
835 (2019) MicroScope-an integrated resource for community expertise of gene functions
836 and comparative analysis of microbial genomic and metabolic data. *Brief Bioinform* **20**:
837 1071-1084.

838 59. Ledermann, R., Bartsch, I., Remus-Emsermann, M.N., Vorholt, J.A., and Fischer, H.M.
839 (2015) Stable fluorescent and enzymatic tagging of *Bradyrhizobium diazoefficiens* to
840 analyze host-plant infection and colonization. *Mol Plant-Microbe Interact* **28**: 959–967.

841 60. Ducret, A., Quardokus, E. M., & Brun, Y. V. (2016). MicrobeJ, a tool for high
842 throughput bacterial cell detection and quantitative analysis. *Nature Microbiology*, **1**(7),
843 16077.

844 61. Beroual, W., and Biondi, E.G. (2019) A new factor controlling cell envelope integrity
845 in Alphaproteobacteria in the context of cell cycle, stress response and infection. *Mol*
846 *Microbiol.* **111**(3):553-555.

847

848 **Figure legends**

849

850 **Figure 1. The non-adapted symbiotic couple formed by *Bradyrhizobium diazoefficiens***
851 **USDA110 and the NCR-producing plant *Aeschynomene afraspera* displays suboptimal**
852 **nitrogen fixation and nodule metabolic dysfunction.** A. Phylogenetic ML tree of a selection
853 of plant species based on *matK* nucleotide sequences. Red branches indicate clades of legumes
854 plants inducing terminal bacteroid differentiation. Blue boxes indicate the distantly-related host
855 plants used in this study. Bootstrap values are mentioned in green on each node of the tree. B,C.
856 General aspect of the plants and nodule sections (inlays) displaying the red coloration of

857 leghaemoglobin of *G. max* (B) and *A. afraspera* (C) at 14 dpi. Scale bars: 5 cm (plants) and 1
858 mm (nodules). D, E. Nitrogen fixation activity determined by acetylene reduction assay (D) and
859 gain in biomass attributable to the symbiosis (E) of 14 dpi plants. F. Whole-nodule metabolome
860 determined by GC/MS or LC/MS at 14 dpi. Histograms show the average value of the relative
861 metabolite concentration of four biological replicates. Letters represent significant differences
862 after ANOVA and post hoc Tukey tests ($p < 0.05$). GM: *G. max* bacteroids, AA: *A. afraspera*
863 bacteroids, USDA: *B. diazoefficiens* USDA110, ORS: *Bradyrhizobium* sp. ORS285.

864

865 **Figure 2. Experimental setup and general description of the transcriptomics and**
866 **proteomics dataset.** A. Experimental setup displaying the three biological conditions of this
867 study. B. Principal component analysis of the proteomics and transcriptomics datasets. C. Venn
868 diagram representing the overlap between differentially expressed genes (DEGs, FDR < 0.01
869 & $|LFC| > 1.58$) and differentially accumulated proteins (DAPs, FDR < 0.05) in at least one
870 comparison and among the population of detected proteins. D. Pearson correlation coefficient
871 (r) distribution between transcriptomic and proteomic datasets based on DAPs only (red) or
872 DAPs that are also DEGs (green). E. Heatmaps and hierarchical clustering of the 815 DAPs
873 and the corresponding transcriptomic expression values. The heatmaps show the standard score
874 (z-score) of assigned spectra and DESeq2 normalized read counts, respectively. The color-
875 coded scale bars for the normalized expression and value of Pearson correlation coefficient of
876 the genes are indicated below the heatmap. YM: Yeast-Mannitol culture, GM: *G. max*
877 bacteroids, AA: *A. afraspera* bacteroids.

878

879 **Figure 3: Symbiosis and host-specific functions that display congruency between**
880 **transcriptomics and proteomics** A. Heatmap with SOM clustering displaying bacterial
881 functions that are commonly DAP and DEG *in planta* in both host plants as compared to the

882 culture reference. B. Heatmap displaying bacterial functions that are commonly DEG and DAP
883 in one host as compared to the other (upper panel: *A. afraspera* > *G. max*; lower panel: *G. max*
884 > *A. afraspera*). In panels A-B, data are presented as log 2 of DESeq2 normalized read counts
885 (RNA-seq) or spectral counting (Proteomics). YM: Yeast-Mannitol culture, GM: *G. max*
886 bacteroids, AA: *A. afraspera* bacteroids.

887

888 **Figure 4: Expression pattern of *B. diazoefficiens* USDA110 and *Bradyrhizobium* sp.**
889 **ORS285 orthologous genes in planta and in culture.** A. Heatmap after SOM clustering of all
890 the orthologous genes of USDA110 and ORS285 obtained with Phyloprofile. Values present
891 the *in planta* LFC calculated after the read counts of the culture control versus *A. afraspera* 14
892 dpi nodules. B. Heatmaps of the orthologous genes after filtering on the FDR (< 0.01) values.
893 Selected genes are highlighted for each class of interest. C. Dot plot of the orthologous genes
894 that are DEG (FDR < 0.01 and |LFC| > 1.58) *in planta* (ie. in *A. afraspera* nodules) in both
895 strains. The red dashed line is for the linear regression and the blue envelope shows a 0.95
896 confidence interval of the linear regression.

897

898 **Figure 5. *B. diazoefficiens* USDA110 displays atypical bacteroid differentiation features**
899 **in *A. afraspera* nodules.** A. Average cell shape of free-living bacteria and bacteroids
900 determined by MicrobeJ (900 < n < 21 000). B. DNA content of USDA110 bacteroids extracted
901 from soybean and *A. afraspera* determined by flow cytometry. C. Assessment of the
902 permeability of USDA110 and ORS285 free-living cells and bacteroids 20 min after PI
903 treatment. *: wilcoxon test, p-value < 0.01. Five biological replicates were performed for
904 bacteroids and two for free-living bacteria. D. Viability of soybean and *A. afraspera* extracted
905 bacteroids at 14 dpi. Asterisks point out significant differences according to a wilcoxon test. *:
906 p-value < 0.05; **: p-value < 0.01. Data are representative of 10 independent plants.

907

908 **Supplementary figure and table legends**

909

910 **Figure S1. Nitrogen and carbon content in aerial parts of the plants were determined by**
911 **elemental analysis.** GM: *G. max*, AA: *A. afraspera*, ORS: inoculated by *Bradyrhizobium* sp.
912 ORS285, USDA: inoculated by *B. diazoefficiens* USDA110, NI: Non-inoculated plants.

913

914 **Figure S2. Nutritional status of 14 dpi plants determined by the shoot/root mass ratios.**
915 AA: *A. afraspera*, ORS: inoculated by *Bradyrhizobium* sp. ORS285, USDA: inoculated by *B.*
916 *diazoefficiens* USDA110, NI: Non-inoculated plants. Letters represent significant differences
917 after t-test or ANOVA and post hoc Tukey tests ($p < 0.05$).

918

919 **Figure S3. Overview of the 129 quantified metabolites in *G. max* and *A. afraspera* whole**
920 **nodules elicited by *B. diazoefficiens* USDA110 or *Bradyrhizobium* sp. ORS285.** Heatmap
921 and hierarchical clustering of the 129 metabolites that were quantified either by gas- (GC-MS)
922 or liquid-chromatography (LC-MS) coupled to mass spectrometry. Gm: *G. max*, Aa: *A.*
923 *afraspera*, O: inoculated by *Bradyrhizobium* sp. ORS285, U: inoculated by *B. diazoefficiens*
924 USDA110.

925

926 **Figure S4. General overview of the datasets using COG classification.** Repartitions of the
927 assigned spectra (left panel) and normalized reads (right panel) among COG classes in the three
928 conditions (blue: bacterial culture, ocher: *B. diazoefficiens* USDA110 in *G. max* nodules, green:
929 *B. diazoefficiens* USDA110 in *A. afraspera* nodules).

930

931 **Figure S5. Western blot analysis of selected USDA110 proteins in culture and in**
932 **bacteroids.** NifH protein were analyzed by western blots on purified USDA110 bacteroids
933 extracted from soybean and *A. afraspera* nodules 14 dpi. Exponential and stationary phase
934 cultures were used as controls.

935

936 **Figure S6. Analysis of cellular differentiation using automated morphometry. A, B, C &**
937 D. Parameters were quantified by image analysis of syto9 stained bacteria and bacteroids using
938 MicrobeJ. The process from raw images (A), segmentation (B), object detection (C) and
939 measurements (D) is depicted with these four panels. E. Cell area. F. Cell width. G. Cell length.

940

941 **Figure S7. Kinetic analysis of bacterial membrane permeability.** Kinetics of propidium
942 iodide uptake assays (reflecting membrane permeability) from which data presented in Figure
943 5C were extracted. The PI permeability was measured by flow cytometry over 60 min after
944 treatment on *A. afraspera* nodule extracted USDA110 (AaU) or ORS285 (AaO) bacteroids and
945 *G. max* extracted USDA110 bacteroids at 14 dpi (GmU). Exponential phase bacterial culture
946 of USDA110 and ORS285 where used as controls. Each dot represent three independent
947 measures and error bars represent the standard deviation of the samples.

948

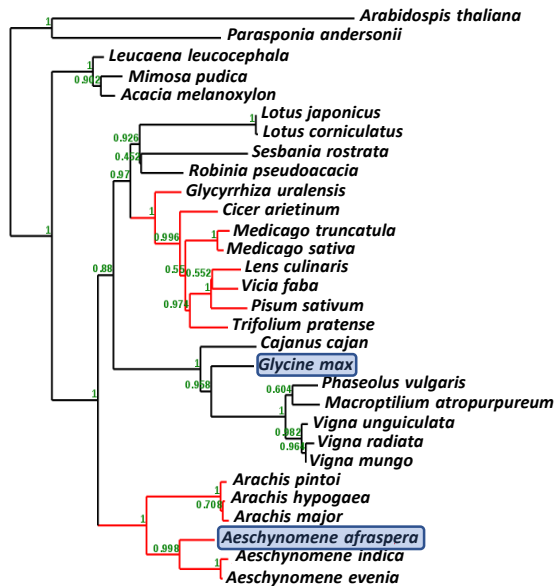
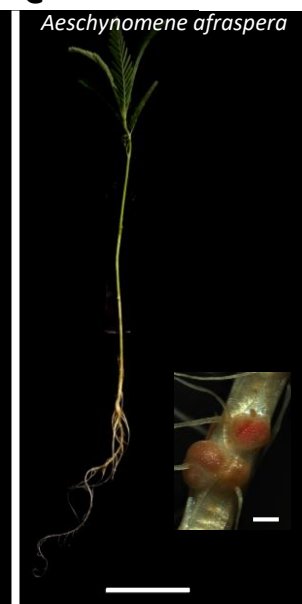
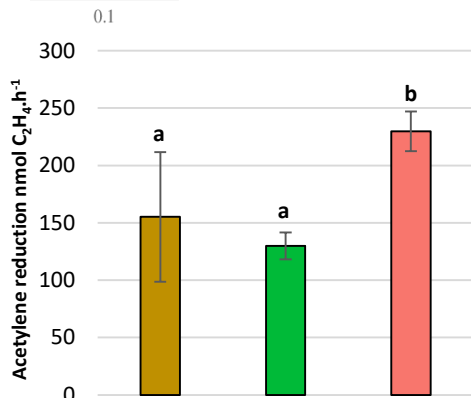
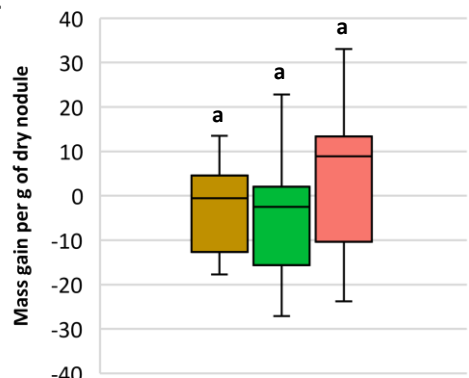
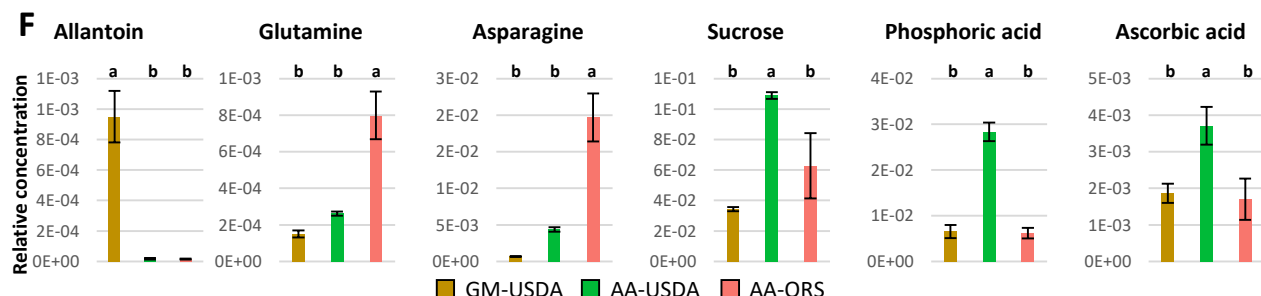
949 **Table S1. Genome annotation, transcriptomic and proteomic data of *B. diazoefficiens***
950 **USDA110 generated in this study.** Description of proteomic and transcriptomic data of
951 USDA110 related conditions. DESeq2 normalized reads, false discovery rate (FDR) values as
952 well as log2 fold change (LFC) are used to describe transcriptomic data. On the other side,
953 spectral counting (SC) along with related statistical indicators, Tukey statistical test result and
954 p-value depict the proteomic data.

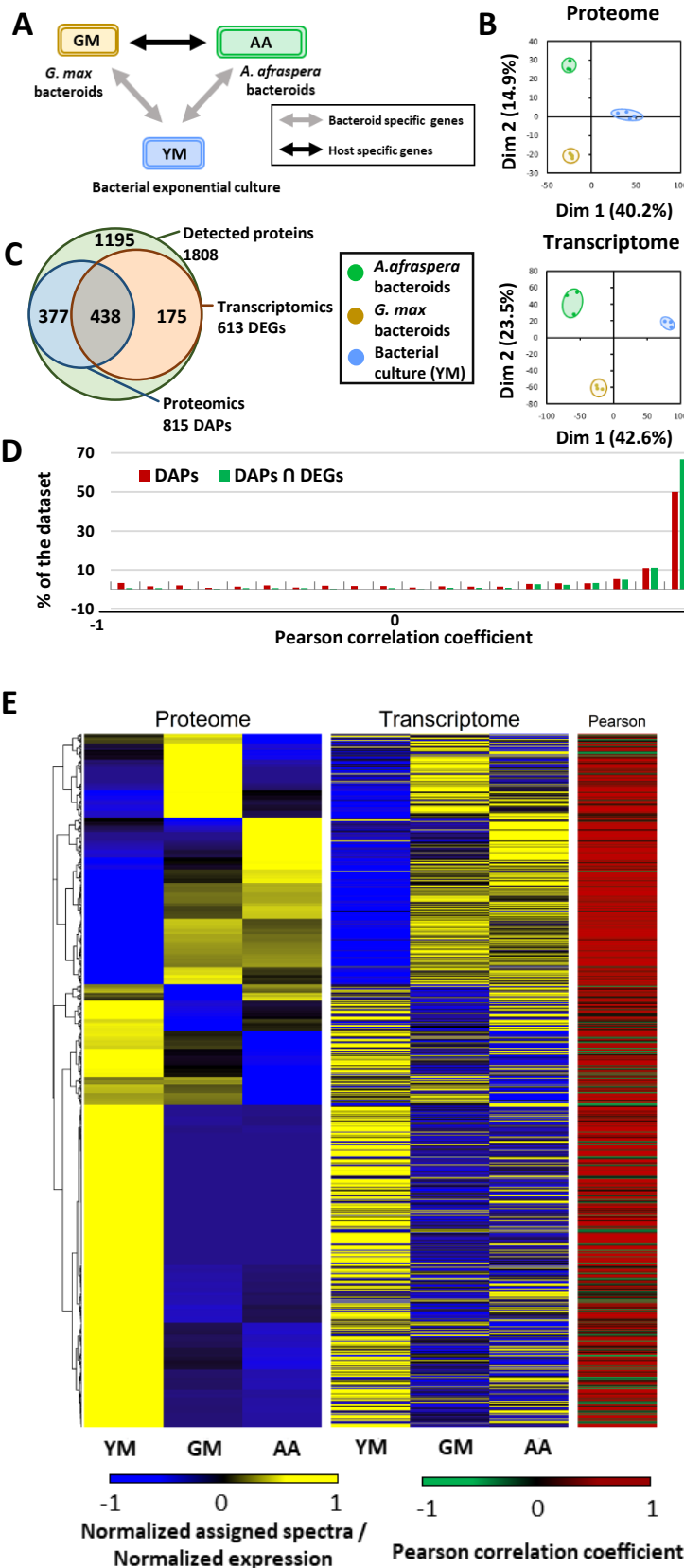
955

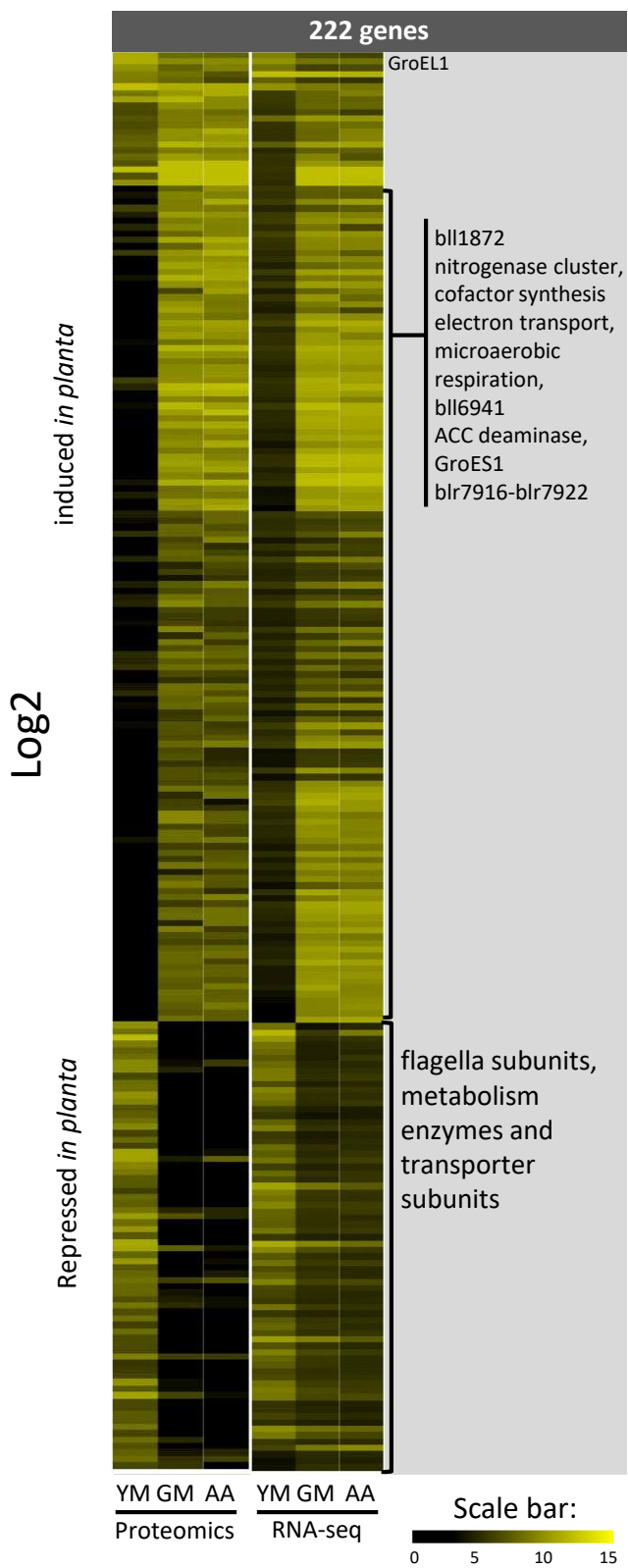
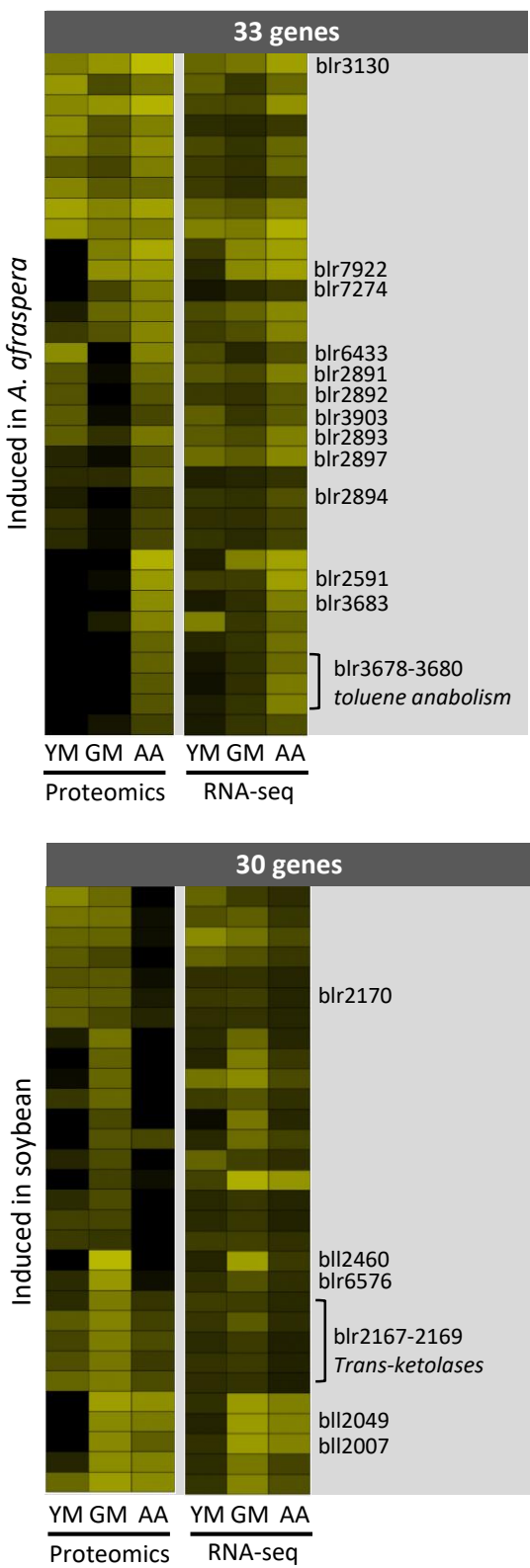
956 **Table S2. Expression analysis of selected *B. diazoefficiens* USDA110 regulons and**
957 **stimulons.** Detailed analysis of the previously determined regulons and stimulons of USDA110
958 based on our transcriptomic data. A given regulon/stimulon was considered differentially
959 regulated when $\geq 40\%$ of the corresponding genes were differentially expressed in our
960 conditions.

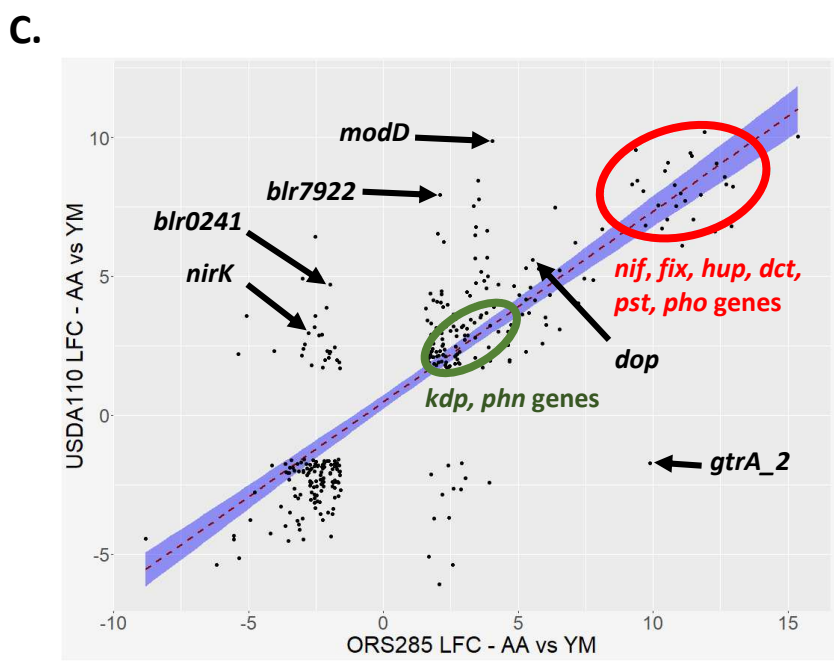
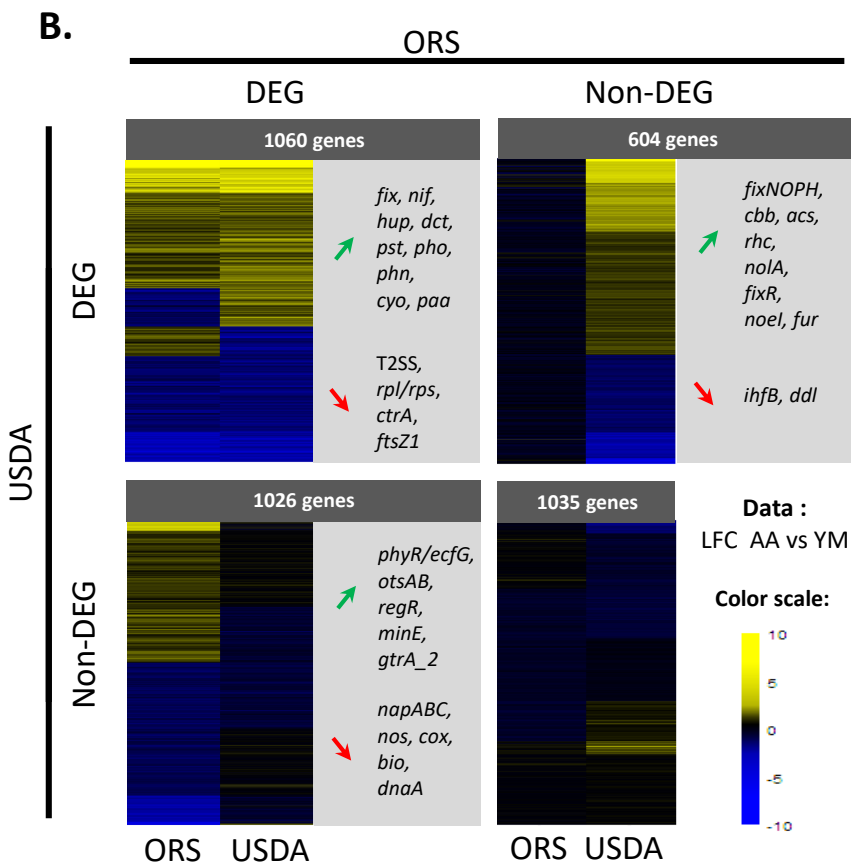
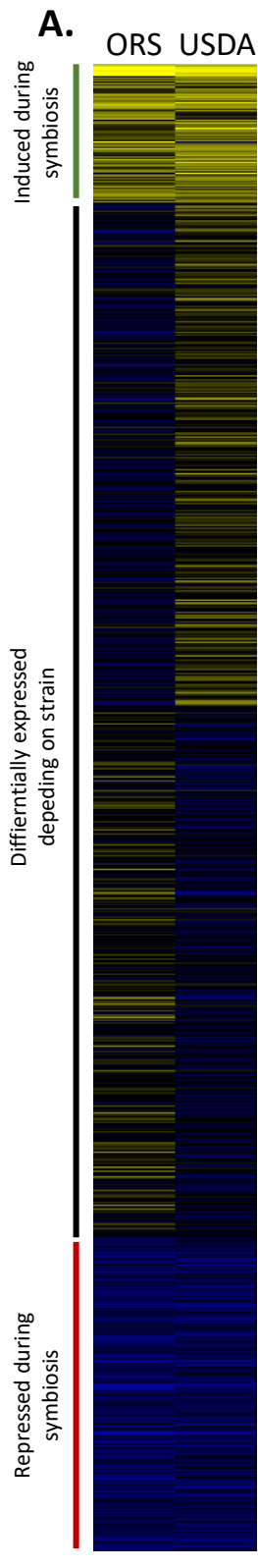
961

962 **Table S3. List of the 3725 orthologous genes shared by *B. diazoefficiens* USDA110 and**
963 ***Bradyrhizobium* sp. ORS285 with their corresponding expression level in rich medium and**
964 **in *A. afraspera* nodules.** This dataset was obtained after a Phyloprofile analysis on Mage
965 Microscope website and was used to generate the Figure 4. Normalized read counts are shown
966 together with the corresponding LFC and FDR as determined by DESeq2.

A**B****C****D****E****F**



A.**B.**



LFC AA vs YM

